Tephra deposition and bonding with reactive oxides enhances burial of organic carbon in the Bering Sea

Jack Longman[1, 2, *] (ORCID: 0000-0002-2725-2617), Thomas M. Gernon[2] (ORCID: 0000-0002-7717-2092), Martin R. Palmer[2], Hayley R. Manners[2,3] (ORCID: 0000-0001-8545-4463).

[1]Marine Isotope Geochemistry, Institute for Chemistry and Biology of the Marine Environment (ICBM), University of Oldenburg, 26129 Oldenburg, Germany

[2]School of Ocean & Earth Science, University of Southampton, Southampton SO14 3ZH, UK

[3]School of Geography, Earth and Environmental Sciences, University of Plymouth, Plymouth, PL4 8AA, United Kingdom

[*] Corresponding author: Jack Longman: jack.longman@uni-oldenburg.de

Key Points

- Tephra layers are loci of marine organic carbon (OC) burial with distinct carbon isotopic compositions.
- Preservation primarily linked to association of OC with reactive iron phases, accounting for ~80% of all OC in tephra layers.
- Distribution of reactive iron from tephras into surrounding sediment has enhanced OC burial in these layers (~33% of OC in sediments bound to reactive phases).
- OC-reactive Fe coupling is observed in sediments >700,000 years old, indicating long-term persistence of these complexes.
- These interactions may help explain how OC is preserved in sediments on geological timescales.

Abstract

Preservation of organic carbon (OC) in marine sediments exerts a major control on the cycling of carbon in the Earth system. In these marine environments, OC preservation may be enhanced by diagenetic reactions in locations where deposition of fragmental volcanic material called tephra occurs. While the mechanisms by which this process occurs are well understood, site-specific studies of this process are limited. Here, we report a study of sediments from the Bering Sea (IODP Site U1339D) to investigate the effects of marine tephra deposition on carbon cycling during the Pleistocene and Holocene. Our results suggest that tephra layers are loci of OC burial with distinct $\delta^{13}C$ values, and that this process is primarily linked to bonding of OC with reactive metals, accounting for ~80% of all OC within tephra layers. In addition, distribution of reactive metals from the tephra into non-volcanic sediments above and below the tephra layers enhances OC preservation in these sediments, with ~33% of OC bound to reactive phases. Importantly, OC-Fe coupling is evident in sediments >700,000 years old. Thus, these interactions may help explain the observed preservation of OC in ancient marine sediments.

Plain Language Summary

The burial of organic carbon in marine sediments is one of the major carbon sinks on Earth, meaning that it removes carbon dioxide from the ocean-atmosphere system. However, the speed at which burial occurs varies across the globe, and is dependent on a range of factors, from the amount of nutrients in the water column, to the type of sediment. Despite evidence suggesting that when tephra is deposited to the seafloor carbon burial is enhanced, very little work has been done to investigate this process. We have therefore analyzed sediments from the Bering Sea, where volcanoes from the Aleutian Islands and Kamchatka regularly deposit tephra in the ocean. We found that organic carbon burial is indeed associated with ash deposition, and importantly, that organic carbon is preserved in the ash layers themselves. We show here that this carbon is preserved effectively because of chemical reactions between the organic carbon and reactive iron, which is released by the ash, creating conditions which preserve carbon for hundreds of thousands of years.

Introduction

The preservation of organic carbon (OC) in marine sediments exerts a controlling influence on the carbon cycle, providing a link between the active pools (e.g. oceans, atmosphere and terrestrial environments) and the inactive, long-term carbon pools, such as those within sedimentary rocks (Arndt et al., 2013; Burdige, 2007; LaRowe et al., 2020). Only about 0.5% of all organic matter produced in the oceans is ultimately preserved in the sedimentary record, with the remainder remineralised and reintroduced into active carbon pools (Hedges & Keil, 1995). The process of OC burial and preservation leads to net removal of CO_2 from the atmosphere, thus any process which changes the marine sedimentary carbon sink is critically important for understanding the climate system on geological timescales.

Explosive volcanism delivers approximately 1 km^3 of ash to the atmosphere every year (Pyle, 1995), and because a high proportion of volcanoes are located close to the oceans, and 70% of the world is covered by oceans, much of this material falls into seawater and onto seafloor substrates (Olgun et al., 2011; Pyle, 1995). Tephra also enters the oceans through rapid erosion of newly created volcanic deposits (Cashman et al., 2013). This material eventually settles to the seafloor, and is deposited in the sedimentary record as tephra layers (Dingwell et al., 2012; Pyle, 1989). Tephra may also derive

from submarine eruptions, such that tephra is thought to represent as much as 25% of marine sediments in the Pacific Ocean (Scudder et al., 2009; Straub & Schmincke, 1998).

There are four mechanisms by which enhanced preservation of OC in marine sediments may occur as a result of tephra deposition and diagenesis: (1) fertilization; (2) reactive metal bonding; (3) reduced oxidant exposure, and (4) authigenic carbonate formation (Longman et al., 2019, 2020). Upon deposition in the ocean, and as a result of the dissolution of reactive mineral phases, tephra releases large amounts of macro- and micronutrients such as P, Fe and Mn (Frogner et al., 2001; Jones & Gislason, 2008) that may alleviate deficiencies (Moore et al., 2013), particularly when Fe is the limiting nutrient. Indeed, the fertilization effect has been observed in the form of phytoplankton blooms in the aftermath of tephra deposition events (Achterberg et al., 2013; Duggen et al., 2010; Langmann et al., 2010; Uematsu et al., 2004). Tephra deposition on the seafloor rapidly reduces pore water O_2 contents to near-zero as a result of oxidation of silicate-bound Fe^{II} (Haeckel et al., 2001; Hembury et al., 2012), thus inhibiting the oxidation and remineralization of OC.

Reactive metal bonding is thought to account for ~20% of all OC preserved in marine sediments (Lalonde et al., 2012), and reactive Fe, Mn and Al phases are known to be released from tephra layers to adjacent sediments during diagenesis (Homoky et al., 2011). Hence, while it has yet to be directly observed, tephra deposition likely also contributes enhanced OC preservation through this process.

The association of abundant tephra layers and high OC concentrations has been taken to suggest that tephra diagenesis played a role in enhanced OC preservation in ancient environments (Lee et al., 2018; Tang et al., 2020), and there is growing evidence of tephra-related processes actively enhancing OC preservation in modern sediments (Hembury et al., 2012; Homoky et al., 2011; Murray et al., 2018). Nevertheless, the role of reactive metals released by tephra in this process has not been studied in detail.

Here, we estimate the contribution of this process, and the others outlined above, to the preservation of OC in the Bering Sea. Our work investigates the changing chemistry above, below and within, tephra layers deposited throughout the Quaternary Period (2.6 Ma to present), helping to improve our understanding of the impact tephra deposition has on marine sedimentary organic carbon.

Methods and Materials

Study Site

Sediments from IODP Expedition 323 site U1339D (54°31.26'N, 169°44.35'W, 200 mbsl), on the Umnak Plateau in the Bering Sea (Fig. 1) largely comprise two lithological end-members: biogenic diatom-rich sediment and a tephra. The volcanogenic material is sourced from eruptions along the Aleutian arc, and constitutes ~4 – 40% of the sediment (Takahashi et al., 2011; Vaughn & Caissie, 2017). Tephras were identified on-ship by their difference in colour (typically black) with respect to the adjacent sediments, abrupt lower and upper contacts, and the presence of glass shards in smear slides (Takahashi et al., 2011). After visual identification of cores, subsampling of both tephra layers and background sediment was undertaken in this study. The surface of the split-core sections was removed and care was taken to ensure that only the centre of the tephra layers was sampled to reduce contamination from the adjacent sediments below visibly detectable levels. In all studied examples, a sharp boundary between background sediment and the base of the tephra layer is present (e.g., Figs. S1-S2). Mixing of sediment into the top of the tephra is present in some tephras,

but this is clearly apparent in the core and, where present, was typically limited to the uppermost 2-3 cm of tephra layers (Figs. S1-S2).

For this study, we selected 9 sections, which are denoted Sections 1 to 9, with their depths and approximate ages indicated in Figure 2 (see Table S1 for details). Indicative ages were taken from the biostratigraphic age model of Takahashi et al. (2011b), interpolating linearly between the midpoint of each datum (see Fig. 2, Table S1).

Geochemical Analyses

Organic Carbon

Organic carbon measurements were carried out on a Vario PYRO cube Element Analyser (EA) coupled to a vision isotope ratio mass spectrometer (IRMS) at the University of Southampton. Approximately 20 mg of homogenised sample was acidified in perchloric acid to remove any carbonate prior to multiple rinses with Milli-Q water. EA quality control was performed via repeated measurements of High Organic Sediment Standard (HOSS; Element Microanalysis Ltd., n=11), with a reproducibility of ±0.07 wt %, and Acetalinide (n=8), with a reproducibility of ±0.1 wt % (1 SD).

Bulk sediment carbon isotope signatures ($\delta^{13}C_{Bulk}$) were measured on CO_2 evolved from EA combustion, and calibrated to USGS 40 and USGS 41a, with reproducibility of ±0.02 ‰ (n=5), and ±0.36 ‰ (n=4), respectively (1 SD). Repeat analyzes of HOSS (n=11), and Acetanilide (n=8) were used for quality control, with precision of ±0.04 ‰ and ±0.05 ‰ respectively (1 SD).

Inorganic Carbon

Approximately 20 mg of homogenised sediment was analyzed via coulometry of perchloric acid treatment-released CO_2, using an AutoMate Prep Device (AutoMate FX, Inc., Bushnell, Florida, USA) using a UIC CM5015 CO_2 Coulometer (UIC Inc., Joliet, Illinois, USA) at the University of Southampton. Calibration was performed using a pure carbonate standard (CAS #471-34-1), and quality control was completed via analysis of an in-house stream sediment standard.

Subsamples of layers which contained quantifiable levels of $CaCO_3$ were then selected for carbonate carbon and oxygen isotope analysis. According to the $CaCO_3$ content, between 5-15 mg of sample was analysed via a Thermo Scientific Kiel IV Carbonate device coupled to a MAT253 IRMS at the University of Southampton. Perchloric acid released CO_2, which was analysed for carbon and oxygen isotopes ($\delta^{13}C_{Carb}$ and $\delta^{18}O$). Replicate analyses of an in-house standard were calibrated to NBS-18 and NBS-19, with reproducibility of ±0.13 ‰ and ±0.12 ‰ for $\delta^{13}C_{Carb}$, and ±0.17 ‰ and ±0.23 ‰ for $\delta^{18}O$ (all 1 SD).

Elemental Geochemistry

Bulk sample geochemistry was carried out after digestion at 130°C for 24 hours via a closed-vessel mixed acid (HNO_3-HCl-HF) approach. Digests were then diluted to 2% HNO_3 and analyzed on a Thermo Scientific X-Series ICP-MS at the University of Southampton. Here, we present data for Al, Mn, Fe and Ba (Table S1). Alongside samples, blanks and reference material (HISS-1 and JMS-1 marine sediment standards) were prepared and analyzed in the same manner (see Table S2 for HISS-1 recoveries and blank values).

Reactive Oxides

To isolate reactive oxide phases, a 4 hour dithionite extraction was performed (Kostka & Luther, 1994; Lalonde et al., 2012; Mehra & Jackson, 1958). Despite the potential drawbacks of this approach, which include incomplete extraction of all OC bound to reactive phases (Fisher et al., 2020), it remains the most widely utilised method for investigating interactions between reactive phases and OC (Faust et al., 2021; Fisher et al., 2021).

For each sample, 4 ml of dithionite reagent (buffered to pH 4.8) was prepared, and added to 0.1 g of homogenised, freeze-dried sediment. To maintain pH 4.8, a buffered 0.35M sodium acetate, 0.2M sodium citrate solution was used, and heated to 60°C in a water bath. Samples were agitated using a vortex mixer every 15 minutes. This approach has been previously used to extract amorphous Fe-oxides alongside a fraction of crystalline Fe-oxides and acid volatile sulphides (Kostka & Luther, 1994; Roy et al., 2013). Dithionite-extracted fractions were diluted in the same manner as for elemental analysis and analyzed on a Thermo Scientific X-Series ICP-MS at the University of Southampton. Results are presented in Table S3. Chilean Margin sediment (RR9702A-42MC, see Muratli et al., (2012)), was prepared and analzsed in the same manner as the samples, with results for reactive Fe (Fe_R) and reactive Mn (Mn_R) found to be within the range of previously reported values (Table S2). For Fe_R, values of 10475±125 ppm (1 SD, n=3) are close to previously measured values of 10800±800 ppm (Roy et al., 2013) and 9300±200 ppm (N.A. Murray et al., 2016). For Mn_R, measured values of 306±15 ppm (1SD, n=3) compare well with other studies, including 290±10 ppm (Murray et al., 2016), and 300±60 ppm (Roy et al., 2013) (Table S2).

To investigate the composition of carbon associated with the phases extracted via dithionite leaching, we used the approach of Lalonde et al. (2012). This involves analysis of the OC content before and after the extraction experiment outlined above, and analysis of $\delta^{13}C_{bulk}$ before and after extraction. In addition, a control experiment was completed, where samples were extracted using sodium chloride instead of sodium dithionite and trisodium citrate, according to the method of Lalonde et al., (2012). For tephra, this released 0.004 wt% of the OC, and for sediment 0.02 wt%. These values were then used to correct experimental data (Lalonde et al., 2012; Shields et al., 2016), although it has been shown this approach can result in underestimations of Fe_R-associated OC (Fisher et al., 2020) (Table S4). For simplicity, and in a similar manner to previous studies (e.g. Faust et al., 2021), we consider the results of the extraction experiment to represent Fe_R-bound OC, and not Mn_R- and Al_R-bound OC. Results are presented in Table S4.

Using the results of the extraction experiment and control experiment, the fraction of OC associated with reactive phases (hereafter $f_{OC\text{-}Fe}$) and the isotopic composition of this OC (hereafter $\delta^{13}C_{Fe\text{-}OC}$) were calculated using the following equation (Lalonde et al., 2012):

$$f_{Fe-OC} = \frac{OC_{extract} - OC_{control}}{OC_{bulk}}$$

where $f_{OC\text{-}Fe}$ is the fraction of OC bound to reactive phases, $OC_{\text{-}control}$ is the OC content after control extraction (for either tephra or sediment), $OC_{\text{-}extract}$ is OC content after dithionite extraction and $OC_{\text{-}bulk}$ is OC content prior to extraction. Using the precision data derived from the EA standards (±0.07 wt %), and the average wt % OC content of the samples lost during the extraction (0.32 wt%), we estimate the error on $f_{OC\text{-}Fe}$ to be on average ±21%. Only two samples display an absolute OC loss lower than the analytical error (Table S3). The isotopic composition of the fraction of OC extracted ($\delta^{13}C_{Fe\text{-}OC}$) was calculated using the following equation:

$$\delta^{13}C_{Fe-OC} = \frac{\delta^{13}C_{bulk} \times OC_{bulk} - \delta^{13}C_{Fe-OC-extract} \times OC_{extract}}{OC_{bulk} - OC_{extract}}$$

where $\delta^{13}C_{bulk}$ is the $\delta^{13}C$ of OC before the dithionite experiment and $\delta^{13}C_{Fe\text{-}OC\text{-}extract}$ is the $\delta^{13}C$ of OC after the dithionite extraction. Using the calculated $\delta^{13}C_{Fe\text{-}OC}$, and the absolute amount of OC associated with Fe_R (OC_{Fe}), the isotopic composition of the non Fe_R-bound OC ($\delta^{13}C_{Non\text{-}Fe\text{-}OC}$) was then calculated using the following equation:

$$\delta^{13}C_{Non-Fe-OC} = \frac{\delta^{13}C_{Fe-OC} \times OC_{Fe} - \delta^{13}C_{bulk} \times OC_{bulk}}{OC_{Fe} - OC_{bulk}}$$

Using a similar approach to that outlined above, precision from IRMS standards (±0.13 ‰), the average $\delta^{13}C_{Fe\text{-}OC}$ (0.56 ‰), we calculate error on $\delta^{13}C_{Fe\text{-}OC}$ estimates to be on average ±22%. In this case, only one sample displays a $\delta^{13}C$ shift lower than analytical error (Table S3).

Palaeoproductivity

To assess changing palaeoproductivity, we used the biogenic fraction of barium (Ba_{Bio}), a commonly used proxy (Schoepfer et al., 2015). This approach first calculates the proportion of excess Ba in the sediments, an approach which uses the expected ratio of Ba to the conservative element Al in detrital, non-biogenic Ba to calculate the remainder:

$$Ba_{Bio} = Ba_{Total} - Al_{Total} \times (Ba/Al_{detrital})$$

For $Ba/Al_{detrital}$, we assume the primary detrital contributor is tephra and use an average value from all tephra layers in this study (0.0099). Using published biostratigraphic ages (Takahashi, Ravelo, & Alvarez Zarikian, 2011), we calculate accumulation rates which are then used to convert raw Ba_{Bio} into Ba_{Bio} flux:

$$Ba_{Bio}Flux = Ba_{Bio} \times \rho \times LSR$$

where LSR is the linear sedimentation rate, in cm^{-1} kyr and ρ is the density of sediment, estimated using the following equation:

$$\rho = 0.0794 \times \ln(x) + 0.650$$

where *x* is the age of the sample in kyr (Schoepfer et al., 2015). Results may be found in Table S1.

Results

The composition of the tephra layers and adjacent non-volcanogenic sediments are compared in Table 1. The tephra layers show lower average OC and inorganic carbon contents, but extend to much higher inorganic carbon concentrations in Section 6 (Fig. 2). The bulk $\delta^{13}C$ values of the two groups overlap, but the tephra layers have more negative mean $\delta^{13}C$ values (-25.4±1.18‰, 1SD, n=22) than those of the sediments (-23.91±0.6‰, 1SD, n=44) (Table S5). The tephra layers are slightly enriched in total Fe and Mn with similar levels of Al to sediment. The tephras contain slightly lower reactive phase contents (Fig. 3; Table 1). The dithionite extraction experiment shows a greater average $f_{OC\text{-}Fe}$ in tephras (79±13%, 1SD, n=13) than sediments (33±22%, 1SD, n=24), with $\delta^{13}C_{Fe\text{-}OC}$ in tephras and sediments averaging -25.83‰ and -24.16‰, respectively (Table 1; Fig. 4, Table S4). Carbonate $\delta^{13}C$ analyses show two clusters for $\delta^{13}C_{Carb}$ (Fig. 5). One cluster (n=5) displays a narrow range in $\delta^{13}C_{Carb}$ values between -1.01 and -1.58 ‰. The other (n=8) has $\delta^{13}C_{Carb}$ values between -13.41 and -19.56 ‰. $\delta^{18}O$ values also differ between the two clusters, with samples in the first lying between -7.09 and 1.34 ‰ and the second between 2.92 and 9.2 ‰ (Fig. 5).

Discussion

OC in tephra layers

Our analyses show that all tephra layers contain a component of OC, with an average of 0.3±0.7 wt% (1SD, n=22), compared to an average of 0.9 wt% in the background sediments (Fig. 2a, Table S5). Because fresh tephra contains negligible OC, these data indicate that some OC preservation mechanism occurred within the tephra layers. Bulk carbon isotope analyses of the tephra layers and surrounding sediments indicate that the composition of this OC is different to what is preserved in surrounding sediments. Mean tephra $\delta^{13}C$ is -25.4±1.2‰ (1SD, n=22) and mean sediment $\delta^{13}C$ is -23.9±0.6‰ (1SD, n=44) (Fig. 2d), with statistically different means and variances (T-test p-value <0.005). This suggests that the tephra layers contain a distinct source of ^{13}C-depleted carbon, which is consistent with the fact that we minimized sampling of any background sedimentary OC mixed into the tephra layers, despite the bioturbated nature of some sediments at site U1339D. However, where present, the effect of bioturbation on tephra is limited to the uppermost 1-2 cm of the layers (Takahashi et al., 2011). Therefore, our sampling method—which avoided gradational boundaries and sampled the centre of the tephras—deliberately avoided the sampling of any potentially mixed sediment (Figs. S1-2). Further, if bioturbation were to have played a role, one would expect the tephra layers to contain a mix of OC brought in from surrounding layers, rather than a distinct source as we observe. It is possible the distinct $\delta^{13}C$ represents a shift to OC of a more terrestrial origin in tephras, with Yukon River OC typically on the order of -27‰ (Guo & Macdonald, 2006). However, this is unlikely to constitute a significant proportion of the OC supply to our site, with the Yukon delta located nearly 1000 km to the northeast. In addition, there is no a priori reason to expect the tephra layers to contain more terrestrial OC than the sediments, but the possibility cannot be discounted.

An additional explanation for the distinct OC $\delta^{13}C$ values in the tephra may be autochthonous microbial biomass formation, because microbial fatty acid $\delta^{13}C$ values range from -30 to -45 ‰, depending on the carbon source (Cifuentes & Salata, 2001; Gong & Hollander, 1997; Hayes, 2001). This occurs due to fractionation processes which take place as microbes utilise carbon, the majority of which result in $\delta^{13}C$ depletion (Hayes, 2001). While we cannot be certain of a biomass origin, the negative values of microbial biomass means that only a relatively small contribution is necessary to result in the observed isotopic shift. Further study would be required to confirm this hypothesis, but evidence suggests that volcanic glass may provide the ideal substrate for microbial growth (Li et al., 2020; Zhang et al., 2017). Indeed, tephra layers have been shown to contain microbial communities which are distinct, more diverse and greater in number than surrounding sediments (Inagaki et al., 2003), with sulfide oxidation suggested as an energy source (Böhnke et al., 2019). However, even if microbial biomass plays a role in the OC preserved in these tephras, both the lack of direct evidence, and the relatively un-depleted $\delta^{13}C$ values in tephra suggest that another source of OC is also present within the tephra layers. One further possibility is that the shift in lithology from sediment to tephra has allowed for the preferential preservation of certain organic compounds, due to changing reactivity and chemical compositions. This could be linked to the preservation of OC via bonding with reactive iron (Fe_R) phases, as a result of the high Fe_R content in ash (Homoky et al., 2011), and there is evidence to suggest that Fe is released during tephra alteration (Luo et al., 2020; Maters et al., 2017). Such a mechanism is not dependent on the formation mechanism of the OC, rather increasing preservation across all OC forms, as the complexes formed are difficult to break down (Lalonde et al., 2012). This may result in the depletion of $\delta^{13}C$ in the tephras, as OC degradation tends to result in the retained OC containing a more negative $\delta^{13}C$ value (Lehmann et al., 2002; Zonneveld et al., 2010), but further research is necessary to confirm this. As such, it may be that the OC retained in the tephra is simply marine OC which has undergone selective preservation, resulting

in more depleted $\delta^{13}C$ than surrounding sediment (Fig. 4). Thus, a microbial component cannot be discounted, but also cannot be proven from our data alone.

Reactive metal bonding

Globally, ~20% of marine OC is thought to be preserved via bonding with Fe_R phases (Barber et al., 2017; Lalonde et al., 2012), hence we have investigated how bonding reactions may have influenced OC preservation at U1339D. Absolute values of OC associated with Fe (OC-Fe) are similar for both tephra (average 0.31 wt %) and sediment (average 0.27 wt %), but with much more variability in the tephra layers (Fig. 4c; Figure S3). However, the variability in the bulk OC content, and the lower OC content of tephras, means that the percentage of OC associated with FeR ($f_{OC\text{-}Fe}$) is clearly different between the tephra and background sediment (Fig. 4e, Table 1). The $f_{OC\text{-}Fe}$ in the background sediment (average 33%) is similar to the global average, but within the tephra layers, $f_{OC\text{-}Fe}$ increases to an average of 79% (Fig. 4; Table 1). By comparison, the highest $f_{OC\text{-}Fe}$ observed in marine sediments elsewhere is ~40% in deltaic sediments and ~30% in sediments underlying the equatorial Pacific upwelling zone (Lalonde et al., 2012). The intense Fe_R-OC bonding within the tephra layers may be linked to the high proportion of Fe^{II} within tephra deposits (Homoky et al., 2011), that provides an ideal environment for OC inner-sphere bonding (Barber et al., 2017). Interestingly, the Fe_R content of the tephra layers at Site U1339C is lower than those in the background sediments (Fig. 3), potentially because Aleutian eruptions are primarily andesitic and rhyolitic as opposed to basaltic in composition (Figure S4). However, $f_{OC\text{-}Fe}$ is high, supporting recent work which suggests the absolute availability of Fe_R is not the dominant control on OC-Fe association (Faust et al., 2021). The higher proportion of $f_{OC\text{-}Fe}$ in the sediments adjacent to the tephra (relative to the more distal sediments) (Fig. 4) may be related to the diffusion of colloidal reactive Fe out of the tephra layers (cf. Homoky et al., 2011).

The isotopic signature of the Fe_R-bound OC ($\delta^{13}C_{Fe\text{-}OC}$) may indicate the type of OC being preserved via these interactions (Fig 4b, d, f). As with bulk $\delta^{13}C$, the $\delta^{13}C_{Fe\text{-}OC}$ of tephra layers is consistently more negative than those in the sediments, with an average of -25.50 ‰ in tephra, and -22.4 ‰ in sediments (Fig. 4f), suggesting a distinct carbon source. The affinity of marine OC to Fe_R phases has been observed in a range of marine sediments located on the continental shelf previously, likely indicating a marine source of sediment-hosted OC bound to Fe_R (Lalonde et al., 2012), a finding in line with those from other marine environments such as estuaries (Sirois et al., 2018; Zhao et al., 2018). As with bulk sediment OC, it is possible that the more negative nature of $\delta^{13}C_{Fe\text{-}OC}$ in tephras represents a shift toward microbial OC generation and preservation (Cifuentes & Salata, 2001; Gong & Hollander, 1997), resulting from fractionation which occurs as microbes utilise carbon (Hayes, 2001). Circumstantial evidence for this hypothesis comes from laboratory studies which demonstrate that reactive Fe oxides may act as electron suppliers for metabolism of metal-reducing bacteria (Coker et al., 2012; Kato et al., 2010).

However, as with bulk $\delta^{13}C$ values, the variation may result from the preservation of certain OC compounds. Our data appear to support this, as the bulk $\delta^{13}C$ value of tephra is similar to that of tephra-hosted $\delta^{13}C_{Fe\text{-}OC}$ values (Fig. 4), a function of the majority of OC being bound to Fe_R phases in tephra. The retention of a depleted signal in $\delta^{13}C_{Fe\text{-}OC}$ suggests that what remains in the tephra is the non-labile, FeR-complexed OC, and that the loss of labile compounds has caused the depletion. Indeed, in background sediments, $\delta^{13}C_{Fe\text{-}OC}$ displays less negative isotope ratios (Fig. 4). This suggests that outside of tephra layers the isotopic composition has not been shifted as Fe-OC makes up a smaller proportion of total OC and so less preservation of negative $\delta^{13}C$ is occurring. The

enhancement of OC preservation due to Fe_R bonding in tephra layers may thus provide a previously unconsidered sink for such OC in sediments containing abundant tephra (Hedges et al., 1997).

The molar ratio of organic carbon to reactive iron (OC:Fe; Fig. 5a, Table S4) may provide information on the mechanisms of binding between OC and Fe (Faust et al., 2021; Lalonde et al., 2012), with low ratios indicative of simple mono-layer sorption, and higher ratios related to coprecipitation (Wagai & Mayer, 2007). In the Bering Sea sections, OC:Fe molar ratios vary greatly, suggesting a range of OC-Fe interactions, but tephra layers typically display lower OC:Fe than in the surrounding sediments (Fig. 5a). The high OC:Fe ratios observed in some layers (OC:Fe >10) may indicate deposition under anoxic/sub-oxic conditions (Lalonde et al., 2012). In tephra layers, this is likely related to the consumption of porewater O_2 during tephra diagenesis (Hembury et al., 2012). Low OC:Fe ratios are typically linked to O_2 exposure (Lalonde et al., 2012), or terrestrial OC-Fe bonding (Barber et al., 2014; Faust et al., 2021), but as discussed above these mechanisms are unlikely to be at play here. If microbial activity is a contributor to tephra OC, utilisation of the reactive Fe during microbial metabolism may have altered the Fe_R content adsorbed or coprecipitated to other OC (Elizabeth Cooper et al., 2017; Eusterhues et al., 2014). Further, since the dithionite extraction removes all "reactive" Fe phases, and not simply those complexed with OC, it is possible that low OC:Fe ratios are related to the extraction of Fe_R phases not involved with bonding (Faust et al., 2021). By pairing our OC:Fe data with $f_{OC\text{-}Fe}$, and comparing with previous studies, it is clear that the OC-Fe_R interaction in tephra layers differ from any previous studies (Fig. 6). Our sediment data are close to previous studies of oxic and suboxic sediments (Lalonde et al., 2012), but the tephras show very high $f_{OC\text{-}Fe}$ associated with low OC:Fe. This further indicates that a process not typically associated with marine sediments occurs in the tephra layers (Fig. 6).

Long term persistence of an enhanced 'rusty carbon sink' in tephra-rich sediments

Regardless of the source of the OC preserved in the sediments and tephra, there is evidence of extensive OC-Fe_R bonding in all layers of the studied Bering Sea sediments, with particularly high levels of OC complexion in both the tephras and surrounding sediments (Fig. 4). These values suggest that the environment produced by tephra deposition, in which enhanced availability of nutrients (and potentially Fe_R although not in the Bering Sea) is coupled to localised oxygen depletion (Hembury et al., 2012), is one in which high proportions of local OC are complexed to Fe_R. The enhanced $f_{OC\text{-}Fe}$ proportions in tephras are greater than reported in any surface sediments, even in anoxic depositional environments, suggesting the size of the 'rusty sink' in any given sediment may be more related to the availability of Fe_R phases and not the available oxygen (Lalonde et al., 2012).

In addition, even in the oldest layers around the tephra deposited between 700-745 kyr (i.e., section 21H4; Takahashi et al., 2011), all $f_{OC\text{-}Fe}$ proportions are above 10%, and greater than 70% in the tephra. This suggests that bonding with reactive oxides provides a long-term sink for OC in the marine environment, one which persists for far longer than previously indicated (Faust et al., 2021). This has implications for long-term carbon cycling on Earth, suggesting OC-Fe bonding may represent an important component of the high activation energy (*E*) OC involved in the long-term preservation of marine OC (Hemingway et al., 2019). The proportion of high-*E* organic compounds has been shown to increase as time proceeds in marine sediments, with our work suggesting a proportion of this is linked to OC-Fe_R bonds. This finding, coupled with the implication that tephras are loci of intense OC-Fe_R bonding, suggest that tephras may be involved in the burial and long-term

sequestration of OC after periods of major volcanic activity, such as in the Late Ordovician (Buggisch et al., 2010) and the mid-Cretaceous (Lee et al., 2018).

Other processes involved in OC preservation

Another potential carbon sink in tephra is authigenic carbonate (Schrag et al., 2013), which may form in tephra layers themselves (Longman et al., 2021), or sediments in which levels of Ca^{2+} and Mg^{2+} have been enhanced by ash deposition (Hong et al., 2020; Longman et al., 2019; Luo et al., 2020; Torres et al., 2020). In most tephras and sediments at site U1139D, there is little evidence for this process occurring (Fig. 2b), potentially due to the small amount of carbonate precipitation typically promoted by ash alteration (Hong et al., 2020), but there are exceptions, particularly in one layer where carbonate contents exceed 50 wt% (tephra 7; Fig. 2b). In addition, a small number of sediment layers show carbonate enrichment (Fig. 2b).

Carbon and oxygen isotope analyses of the tephra-hosted carbonates ($\delta^{13}C_{Carb}$) indicate that there are two clear groups (Fig. 5b). The first, composed solely of carbonate from sediment layers, is characterized by $\delta^{13}C_{Carb}$ between -1 and -2 ‰, and appears to be indicative of a biogenic carbonate formation, or authigenic carbonates formed from dissolved inorganic carbon in seawater (e.g. Humphreys et al., 2015). The second group shows $\delta^{13}C_{Carb}$ values between -12 to -20 ‰ (Fig. 5b). This ^{12}C depletion is typical of carbonates formed as a result of the anaerobic oxidation of methane once this methane reaches the zone where it occurs in concert with sulfate (Sivan et al., 2007; Whiticar & Faber, 1986). Authigenic carbonates (C_{auth}) formed as a result of this process may act as a carbon sink, preventing the methane from returning carbon to the ocean, and locking it into stable carbonate phases (Schrag et al., 2013). Previous work in the region has shown widespread evidence for C_{auth} in Bering sediment (Pierre et al., 2016), with similarly ^{12}C-depleted carbon isotope signatures (Hein et al., 1979). As we see little evidence for C_{auth} formation in sediments, and with previous work showing C_{auth} in tephra layers (Hein et al., 1979), it is possible that tephra alteration has supplied the Ca^{2+} and Mg^{2+} necessary for formation. If true, this would suggest C_{auth} formation is a carbon sink enhanced by tephra diagenesis.

It is also possible that tephra deposition may stimulate phytoplankton productivity in surface seawater (Langmann et al., 2010; Olgun et al., 2011). Using both OC content and biogenic barium flux (Ba_{Bio}) as proxies for palaeoproductivity (Schoepfer et al., 2015), we investigated the impact of tephra deposition on productivity in the Bering Sea. There is little evidence of increased productivity in sediments directly surrounding tephra deposits, with slightly lower average OC content, and similar Ba_{Bio} (Fig. 2c). This is despite evidence of plankton blooms in the aftermath of eruptions in the region (Hamme et al., 2010; Langmann et al., 2010). This suggests either that: i) plankton blooms are transitory and short-lived, having very little impact on overall productivity in the region; or ii) the organic carbon produced by such blooms is either not exported from the upper ocean prior to remineralisation, or it is transported to other locations by ocean currents. In addition, the Bering Sea is typically an area of high productivity (Wehrmann et al., 2011), so that the addition of tephra makes little difference to overall production. A final possibility is that the andesitic and relatively low-Fe nature of the tephra deposited in the Bering Sea means that it does not contain sufficient amounts of nutrient to influence biological productivity.

Conclusions

Our results demonstrate enhanced OC preservation in tephra, and in the sediments surrounding tephra deposits. The OC in the tephra layers is primarily associated with reactive metal phases, with an average $f_{OC\text{-}Fe}$ value of 77% in tephra. Thus, tephra layers contain the highest $f_{OC\text{-}Fe}$ proportions yet

reported. Isotopic analyses indicate that this OC is primarily marine in origin, supporting previous studies which demonstrate the affiliation of Fe_R to marine OC in marine environments (Sirois et al., 2018; Zhao et al., 2018). The data also shows the viability of long-term stability of such relationships, with high $f_{OC\text{-}Fe}$ proportions in sediments older than 700 kyr. This finding may explain observed increases in OC activation energy as age increases (Hemingway et al., 2019), with OC-Fe_R interactions resulting in hard to break down organic compounds. In addition to bonding of OC with reactive metal phases, there is limited evidence for authigenic carbonate formation in these tephra layers.

References

Achterberg, E. P., Moore, C. M., Henson, S. A., Steigenberger, S., Stohl, A., Eckhardt, S., et al. (2013). Natural iron fertilization by the Eyjafjallajökull volcanic eruption. *Geophysical Research Letters*, *40*(5), 921–926. https://doi.org/10.1002/grl.50221

Arndt, S., Jørgensen, B. B., LaRowe, D. E., Middelburg, J. J., Pancost, R. D., & Regnier, P. (2013). Quantifying the degradation of organic matter in marine sediments: A review and synthesis. *Earth-Science Reviews*, *123*, 53–86. https://doi.org/10.1016/J.EARSCIREV.2013.02.008

Barber, A., Lalonde, K., Mucci, A., & Gélinas, Y. (2014). The role of iron in the diagenesis of organic carbon and nitrogen in sediments: A long-term incubation experiment. *Marine Chemistry*, *162*, 1–9. https://doi.org/10.1016/j.marchem.2014.02.007

Barber, A., Brandes, J., Leri, A., Lalonde, K., Balind, K., Wirick, S., et al. (2017). Preservation of organic matter in marine sediments by inner-sphere interactions with reactive iron. *Scientific Reports*, *7*(1), 366. https://doi.org/10.1038/s41598-017-00494-0

Böhnke, S., Sass, K., Gonnella, G., Diehl, A., Kleint, C., Bach, W., et al. (2019). Parameters Governing the Community Structure and Element Turnover in Kermadec Volcanic Ash and Hydrothermal Fluids as Monitored by Inorganic Electron Donor Consumption, Autotrophic CO2 Fixation and 16S Tags of the Transcriptome in Incubation Experiments. *Frontiers in Microbiology*, *10*, 2296. https://doi.org/10.3389/FMICB.2019.02296

Buggisch, W., Joachimski, M. M., Lehnert, O., Bergström, S. M., Repetski, J. E., & Webers, G. F. (2010). Did intense volcanism trigger the first Late Ordovician icehouse? *Geology*, *38*(4), 327–330. https://doi.org/10.1130/G30577.1

Burdige, D. J. (2007). Preservation of organic matter in marine sediments: Controls, mechanisms, and an imbalance in sediment organic carbon budgets? *Chemical Reviews*, *107*(2), 467–485. https://doi.org/10.1021/cr050347q

Cashman, K. V., Stephen, R., & Sparks, J. (2013). How volcanoes work: A 25 year perspective. *Bulletin of the Geological Society of America*, *125*(5–6), 664–690. https://doi.org/10.1130/B30720.1

Cifuentes, L. A., & Salata, G. G. (2001). Significance of carbon isotope discrimination between bulk carbon and extracted phospholipid fatty acids in selected terrestrial and marine environments. *Organic Geochemistry*, *32*(4), 613–621. https://doi.org/10.1016/S0146-6380(00)00198-4

Coker, V. S., Byrne, J. M., Telling, N. D., Van Der Laan, G., Lloyd, J. R., Hitchcock, A. P., et al. (2012). Characterisation of the dissimilatory reduction of Fe(III)-oxyhydroxide at the microbe - mineral interface: The application of STXM-XMCD. *Geobiology*, *10*(4), 347–354. https://doi.org/10.1111/j.1472-4669.2012.00329.x

Dingwell, D. B., Lavallée, Y., & Kueppers, U. (2012). Volcanic ash: A primary agent in the Earth

system. *Physics and Chemistry of the Earth, Parts A/B/C*, *45–46*, 2–4. https://doi.org/10.1016/J.PCE.2011.07.007

Duggen, S., Olgun, N., Croot, P., Hoffmann, L., Dietze, H., Delmelle, P., & Teschner, C. (2010). The role of airborne volcanic ash for the surface ocean biogeochemical iron-cycle: a review. *Biogeosciences*, *7*(3), 827–844. https://doi.org/10.5194/bg-7-827-2010

Elizabeth Cooper, R., Eusterhues, K., Wegner, C. E., Uwe Totsche, K., & Küsel, K. (2017). Ferrihydrite-associated organic matter (OM) stimulates reduction by Shewanella oneidensis MR-1 and a complex microbial consortia. *Biogeosciences*, *14*(22), 5171–5188. https://doi.org/10.5194/bg-14-5171-2017

Eusterhues, K., Hädrich, A., Neidhardt, J., Küsel, K., Keller, T. F., Jandt, K. D., & Totsche, K. U. (2014). Reduction of ferrihydrite with adsorbed and coprecipitated organic matter: Microbial reduction by Geobacter bremensis vs. abiotic reduction by Na-dithionite. *Biogeosciences*, *11*(18), 4953–4966. https://doi.org/10.5194/bg-11-4953-2014

Faust, J. C., Tessin, A., Fisher, B. J., Zindorf, M., Papadaki, S., Hendry, K. R., et al. (2021). Millennial scale persistence of organic carbon bound to iron in Arctic marine sediments. *Nature Communications*, *12*(1), 1–9. https://doi.org/10.1038/s41467-020-20550-0

Fisher, B. J., Moore, O. W., Faust, J. C., Peacock, C. L., & März, C. (2020). Experimental evaluation of the extractability of iron bound organic carbon in sediments as a function of carboxyl content. *Chemical Geology*, *556*, 119853. https://doi.org/10.1016/j.chemgeo.2020.119853

Fisher, B. J., Faust, J. C., Moore, O. W., Peacock, C. L., & März, C. (2021). Technical note: Uncovering the influence of methodological variations on the extractability of iron-bound organic carbon. *Biogeosciences*, *18*(11), 3409–3419. https://doi.org/10.5194/BG-18-3409-2021

Fisk, M. R., Giovannoni, S. J., & Thorseth, I. H. (1998). Alteration of oceanic volcanic glass: Textural evidence of microbial activity. *Science*, *281*(5379), 978–980. https://doi.org/10.1126/science.281.5379.978

Frogner, P., Reynir Gíslason, S., & Óskarsson, N. (2001). Fertilizing potential of volcanic ash in ocean surface water. *Geology*, *29*(6), 487. https://doi.org/10.1130/0091-7613(2001)029<0487:FPOVAI>2.0.CO;2

Gong, C., & Hollander, D. J. (1997). Differential contribution of bacteria to sedimentary organic matter in oxic and anoxic environments, Santa Monica Basin, California. In *Organic Geochemistry* (Vol. 26, pp. 545–563). Pergamon. https://doi.org/10.1016/S0146-6380(97)00018-1

Hamme, R. C., Webley, P. W., Crawford, W. R., Whitney, F. A., DeGrandpre, M. D., Emerson, S. R., et al. (2010). Volcanic ash fuels anomalous plankton bloom in subarctic northeast Pacific. *Geophysical Research Letters*, *37*(19), n/a-n/a. https://doi.org/10.1029/2010GL044629

Hayes, J. M. (2001). Fractionation of carbon and hydrogen isotopes in biosynthetic processes. *Reviews in Mineralogy and Geochemistry*, *43*(1), 191–277. https://doi.org/10.2138/gsrmg.43.1.225

Hedges, J. I., Keil, R. G., & Benner, R. (1997). What happens to terrestrial organic matter in the ocean? In *Organic Geochemistry* (Vol. 27, pp. 195–212). Pergamon. https://doi.org/10.1016/S0146-6380(97)00066-1

Hedges, John I., & Keil, R. G. (1995). Sedimentary organic matter preservation: an assessment and speculative synthesis. *Marine Chemistry*, *49*(2–3), 81–115. https://doi.org/10.1016/0304-4203(95)00008-F

Hein, J. R., O'Neil, J. R., Jones, O'NEIL, J. R., & JONES, M. G. (1979). Origin of authigenic carbonates in sediment from the deep Bering Sea. *Sedimentology*, *26*(5), 681–705. https://doi.org/10.1111/j.1365-3091.1979.tb00937.x

Hembury, D. J., Palmer, M. R., Fones, G. R., Mills, R. A., Marsh, R., & Jones, M. T. (2012). Uptake of dissolved oxygen during marine diagenesis of fresh volcanic material. *Geochimica et Cosmochimica Acta*, *84*, 353–368. https://doi.org/10.1016/J.GCA.2012.01.017

Hemingway, J. D., Rothman, D. H., Grant, K. E., Rosengard, S. Z., Eglinton, T. I., Derry, L. A., & Galy, V. V. (2019). Mineral protection regulates long-term global preservation of natural organic carbon. *Nature*, *570*(7760), 228–231. https://doi.org/10.1038/s41586-019-1280-6

Homoky, W. B., Hembury, D. J., Hepburn, L. E., Mills, R. A., Statham, P. J., Fones, G. R., & Palmer, M. R. (2011). Iron and manganese diagenesis in deep sea volcanogenic sediments and the origins of pore water colloids. *Geochimica et Cosmochimica Acta*, *75*(17), 5032–5048. https://doi.org/10.1016/J.GCA.2011.06.019

Hong, W. L., Torres, M. E., & Kutterolf, S. (2020). Towards a global quantification of volcanogenic aluminosilicate alteration rates through the mass balance of strontium in marine sediments. *Chemical Geology*, *550*, 119743. https://doi.org/10.1016/j.chemgeo.2020.119743

Humphreys, M. P., Achterberg, E. P., Griffiths, A. M., McDonald, A., & Boyce, A. J. (2015). Measurements of the stable carbon isotope composition of dissolved inorganic carbon in the northeastern Atlantic and Nordic Seas during summer 2012. *Earth System Science Data*, *7*(1), 127–135. https://doi.org/10.5194/essd-7-127-2015

Inagaki, F., Suzuki, M., Takai, K., Oida, H., Sakamoto, T., Aoki, K., et al. (2003). Microbial Communities Associated with Geological Horizons in Coastal Subseafloor Sediments from the Sea of Okhotsk. *Applied and Environmental Microbiology*, *69*(12), 7224–7235. https://doi.org/10.1128/AEM.69.12.7224-7235.2003

Jones, M. T., & Gislason, S. R. (2008). Rapid releases of metal salts and nutrients following the deposition of volcanic ash into aqueous environments. *Geochimica et Cosmochimica Acta*, *72*(15), 3661–3680. https://doi.org/10.1016/j.gca.2008.05.030

Kato, S., Nakamura, R., Kai, F., Watanabe, K., & Hashimoto, K. (2010). Respiratory interactions of soil bacteria with (semi)conductive iron-oxide minerals. *Environmental Microbiology*, *12*(12), 3114–3123. https://doi.org/10.1111/j.1462-2920.2010.02284.x

Kostka, J. E., & Luther, G. W. (1994). Partitioning and speciation of solid phase iron in saltmarsh sediments. *Geochimica et Cosmochimica Acta*, *58*(7), 1701–1710. https://doi.org/10.1016/0016-7037(94)90531-2

Lalonde, K., Mucci, A., Ouellet, A., & Gélinas, Y. (2012). Preservation of organic matter in sediments promoted by iron. *Nature*, *483*(7388), 198–200. https://doi.org/10.1038/nature10855

Langmann, B., Zakšek, K., Hort, M., & Duggen, S. (2010). Volcanic ash as fertiliser for the surface ocean. *Atmos. Chem. Phys. Atmospheric Chemistry and Physics*, *10*, 3891–3899. Retrieved from www.atmos-chem-phys.net/10/3891/2010/

LaRowe, D. E., Arndt, S., Bradley, J. A., Estes, E. R., Hoarfrost, A., Lang, S. Q., et al. (2020, May 1). The fate of organic carbon in marine sediments - New insights from recent data and analysis. *Earth-Science Reviews*. Elsevier B.V. https://doi.org/10.1016/j.earscirev.2020.103146

Lee, C.-T. A., Jiang, H., Ronay, E., Minisini, D., Stiles, J., & Neal, M. (2018). Volcanic ash as a driver of enhanced organic carbon burial in the Cretaceous. *Scientific Reports*, *8*(1), 4197. https://doi.org/10.1038/s41598-018-22576-3

Lehmann, M. F., Bernasconi, S. M., Barbieri, A., & McKenzie, J. A. (2002). Preservation of organic matter and alteration of its carbon and nitrogen isotope composition during simulated and in situ early sedimentary diagenesis. *Geochimica et Cosmochimica Acta*, *66*(20), 3573–3584. https://doi.org/10.1016/S0016-7037(02)00968-7

Li, L., Bai, S., Li, J., Wang, S., Tang, L., Dasgupta, S., et al. (2020). Volcanic ash inputs enhance the deep-sea seabed metal-biogeochemical cycle: A case study in the Yap Trench, western Pacific Ocean. *Marine Geology*, *430*, 106340. https://doi.org/10.1016/j.margeo.2020.106340

Longman, J., Palmer, M. R., Gernon, T. M., & Manners, H. R. (2019). The role of tephra in enhancing organic carbon preservation in marine sediments. *Earth-Science Reviews*, *192*, 480–490. https://doi.org/10.1016/j.earscirev.2019.03.018

Longman, J., Palmer, M. R., & Gernon, T. M. (2020). Viability of greenhouse gas removal via artificial addition of volcanic ash to the ocean. *Anthropocene*, *32*. https://doi.org/10.1016/j.ancene.2020.100264

Longman, J., Gernon, T. M., Palmer, M. R., Jones, M. T., Stokke, E. W., & Svensen, H. H. (2021). Marine diagenesis of tephra aided the Paleocene-Eocene Thermal Maximum termination. *Earth and Planetary Science Letters*, *571*, 117101. https://doi.org/10.1016/J.EPSL.2021.117101

Luo, M., Torres, M. E., Hong, W. L., Pape, T., Fronzek, J., Kutterolf, S., et al. (2020). Impact of iron release by volcanic ash alteration on carbon cycling in sediments of the northern Hikurangi margin. *Earth and Planetary Science Letters*, *541*, 116288. https://doi.org/10.1016/j.epsl.2020.116288

Maters, E. C., Delmelle, P., & Gunnlaugsson, H. P. (2017). Controls on iron mobilisation from volcanic ash at low pH: Insights from dissolution experiments and Mössbauer spectroscopy. *Chemical Geology*, *449*, 73–81. https://doi.org/10.1016/J.CHEMGEO.2016.11.036

Mehra, O. P., & Jackson, M. L. (1958). Iron Oxide Removal from Soils and Clays by a Dithionite-Citrate System Buffered with Sodium Bicarbonate. *Clays and Clay Minerals*, *7*(1), 317–327. https://doi.org/10.1346/CCMN.1958.0070122

Moore, C. M., Mills, M. M., Arrigo, K. R., Berman-Frank, I., Bopp, L., Boyd, P. W., et al. (2013). Processes and patterns of oceanic nutrient limitation. *Nature Geoscience*, *6*(9), 701–710. https://doi.org/10.1038/ngeo1765

Muratli, J. M., McManus, J., Mix, A., & Chase, Z. (2012). Dissolution of fluoride complexes following microwave-assisted hydrofluoric acid digestion of marine sediments. *Talanta*, *89*, 195–200. https://doi.org/10.1016/j.talanta.2011.11.081

Murray, N.A., Muratli, J. M., Hartwell, A. M., Manners, H., Megowan, M. R., Goñi, M., et al. (2016). Data report: dissolved minor element compositions, sediment major and minor element concentrations, and reactive iron and manganese data from the Lesser Antilles volcanic arc

563 region, IODP Expedition 340 Sites U1394, U1395, U1396, U1399, and U1400. *Proceedings of the*
564 *Integrated Ocean Drilling Program*, *340*. https://doi.org/10.2204/iodp.proc.340.207.2016

565 Murray, Natalie A., McManus, J., Palmer, M. R., Haley, B., & Manners, H. (2018). Diagenesis in
566 tephra-rich sediments from the Lesser Antilles Volcanic Arc: Pore fluid constraints. *Geochimica*
567 *et Cosmochimica Acta*, *228*, 119–135. https://doi.org/10.1016/J.GCA.2018.02.039

568 Norrman, B., Zwelfel, U. L., Hopkinson, C. S., & Brian, F. (1995). Production and utilization of
569 dissolved organic carbon during an experimental diatom bloom. *Limnology and Oceanography*,
570 *40*(5), 898–907. https://doi.org/10.4319/LO.1995.40.5.0898

571 Ogawa, H., Amagai, Y., Koike, I., Kaiser, K., & Benner, R. (2001). Production of refractory dissolved
572 organic matter by bacteria. *Science*, *292*(5518), 917–920.
573 https://doi.org/10.1126/science.1057627

574 Olgun, N., Duggen, S., Croot, P. L., Delmelle, P., Dietze, H., Schacht, U., et al. (2011). Surface ocean
575 iron fertilization: The role of airborne volcanic ash from subduction zone and hot spot
576 volcanoes and related iron fluxes into the Pacific Ocean. *Global Biogeochemical Cycles*, *25*(4),
577 n/a-n/a. https://doi.org/10.1029/2009GB003761

578 Pierre, C., Blanc-Valleron, M. M., Caquineau, S., März, C., Ravelo, A. C., Takahashi, K., & Alvarez
579 Zarikian, C. (2016). Mineralogical, geochemical and isotopic characterization of authigenic
580 carbonates from the methane-bearing sediments of the Bering Sea continental margin (IODP
581 Expedition 323, Sites U1343-U1345). *Deep-Sea Research Part II: Topical Studies in*
582 *Oceanography*, *125–126*, 133–144. https://doi.org/10.1016/j.dsr2.2014.03.011

583 Pyle, D. M. (1989). The thickness, volume and grainsize of tephra fall deposits. *Bulletin of*
584 *Volcanology*, *51*(1), 1–15. https://doi.org/10.1007/BF01086757

585 Pyle, D. M. (1995). Mass and energy budgets of explosive volcanic eruptions. *Geophysical Research*
586 *Letters*, *22*(5), 563–566. https://doi.org/10.1029/95GL00052

587 Roy, M., McManus, J., Goñi, M. A., Chase, Z., Borgeld, J. C., Wheatcroft, R. A., et al. (2013). Reactive
588 iron and manganese distributions in seabed sediments near small mountainous rivers off
589 Oregon and California (USA). *Continental Shelf Research*, *54*, 67–79.
590 https://doi.org/10.1016/J.CSR.2012.12.012

591 Schoepfer, S. D., Shen, J., Wei, H., Tyson, R. V., Ingall, E., & Algeo, T. J. (2015). Total organic carbon,
592 organic phosphorus, and biogenic barium fluxes as proxies for paleomarine productivity. *Earth-*
593 *Science Reviews*, *149*, 23–52. https://doi.org/10.1016/J.EARSCIREV.2014.08.017

594 Schrag, D. P., Higgins, J. A., Macdonald, F. A., & Johnston, D. T. (2013). Authigenic carbonate and the
595 history of the global carbon cycle. *Science*, *339*(6119), 540–3.
596 https://doi.org/10.1126/science.1229578

597 Scudder, R. P., Murray, R. W., & Plank, T. (2009). Dispersed ash in deeply buried sediment from the
598 northwest Pacific Ocean: An example from the Izu–Bonin arc (ODP Site 1149). *Earth and*
599 *Planetary Science Letters*, *284*(3–4), 639–648. https://doi.org/10.1016/J.EPSL.2009.05.037

600 Shields, M. R., Bianchi, T. S., Gélinas, Y., Allison, M. A., & Twilley, R. R. (2016). Enhanced terrestrial
601 carbon preservation promoted by reactive iron in deltaic sediments. *Geophysical Research*
602 *Letters*, *43*(3), 1149–1157. https://doi.org/10.1002/2015GL067388

603 Sirois, M., Couturier, M., Barber, A., Gélinas, Y., & Chaillou, G. (2018). Interactions between iron and

organic carbon in a sandy beach subterranean estuary. *Marine Chemistry*. https://doi.org/10.1016/J.MARCHEM.2018.02.004

Sivan, O., Schrag, D. P., & Murray, R. W. (2007). Rates of methanogenesis and methanotrophy in deep-sea sediments. *Geobiology*, *5*, 141–151. https://doi.org/10.1111/j.1472-4669.2007.00098.x

Staudigel, H., Furnes, H., McLoughlin, N., Banerjee, N. R., Connell, L. B., & Templeton, A. (2008, August 1). 3.5 billion years of glass bioalteration: Volcanic rocks as a basis for microbial life? *Earth-Science Reviews*. Elsevier. https://doi.org/10.1016/j.earscirev.2008.04.005

Straub, S. M., & Schmincke, H. U. (1998). Evaluating the tephra input into Pacific Ocean sediments: distribution in space and time. *Geologische Rundschau*, *87*(3), 461–476. https://doi.org/10.1007/s005310050222

Takahashi, K., Ravelo, A., & Alvarez-Zarikian, C. (2011). *Proceedings of the Integrated Ocean Drilling Program: Expedition Reports: Bering Sea Paleoceanography. vol. 323*. College Station, Texas: Integrated Ocean Drilling Program Management International, Inc., for the Integrated Ocean Drilling Program.

Takahashi, K., Ravelo, A. C., & Alvarez Zarikian, C. A. (2011). Site U1339. In *Proceedings of the Integrated Ocean Drilling Program Volume 323* (p. 84). Tokyo: Integrated Ocean Drilling Program Management International, Inc.

Tang, L., Song, Y., Jiang, S., Jiang, Z., Li, Z., Yang, Y., et al. (2020). Organic matter accumulation of the Wufeng-Longmaxi shales in southern Sichuan Basin: Evidence and insight from volcanism. *Marine and Petroleum Geology*, *120*, 104564. https://doi.org/10.1016/j.marpetgeo.2020.104564

Thorseth, I. H., Furnes, H., & Tumyr, O. (1995). Textural and chemical effects of bacterial activity on basaltic glass: an experimental approach. *Chemical Geology*, *119*(1–4), 139–160. https://doi.org/10.1016/0009-2541(94)00098-S

Thorseth, I. H., Torsvik, T., Torsvik, V., Daae, F. L., & Pedersen, R. B. (2001). Diversity of life in ocean floor basalt. *Earth and Planetary Science Letters*, *194*(1–2), 31–37. https://doi.org/10.1016/S0012-821X(01)00537-4

Torres, M. E., Hong, W. L., Solomon, E. A., Milliken, K., Kim, J. H., Sample, J. C., et al. (2020, January 1). Silicate weathering in anoxic marine sediment as a requirement for authigenic carbonate burial. *Earth-Science Reviews*. Elsevier B.V. https://doi.org/10.1016/j.earscirev.2019.102960

Uematsu, M., Toratani, M., Kajino, M., Narita, Y., Senga, Y., & Kimoto, T. (2004). Enhancement of primary productivity in the western North Pacific caused by the eruption of the Miyake-jima Volcano. *Geophysical Research Letters*, *31*(6), n/a-n/a. https://doi.org/10.1029/2003gl018790

Vaughn, D. R., & Caissie, B. E. (2017). Effects of sea-level, sea-ice extent, and nutrient availability on primary production at the Umnak Plateau, Bering Sea (IODP Site U1339) during Marine Isotope Stage (MIS) 5. *Palaeogeography, Palaeoclimatology, Palaeoecology*, *485*, 283–292. https://doi.org/10.1016/J.PALAEO.2017.06.020

Wagai, R., & Mayer, L. M. (2007). Sorptive stabilization of organic matter in soils by hydrous iron oxides. *Geochimica et Cosmochimica Acta*, *71*(1), 25–35. https://doi.org/10.1016/j.gca.2006.08.047

Wallmann, K., Aloisi, G., Haeckel, M., Tishchenko, P., Pavlova, G., Greinert, J., et al. (2008). Silicate weathering in anoxic marine sediments. *Geochimica et Cosmochimica Acta*, *72*(12), 2895–2918. https://doi.org/10.1016/j.gca.2008.03.026

Wehrmann, L. M., Risgaard-Petersen, N., Schrum, H. N., Walsh, E. A., Huh, Y., Ikehara, M., et al. (2011). Coupled organic and inorganic carbon cycling in the deep subseafloor sediment of the northeastern Bering Sea Slope (IODP Exp. 323). *Chemical Geology*, *284*(3–4), 251–261. https://doi.org/10.1016/j.chemgeo.2011.03.002

Whiticar, M. J., & Faber, E. (1986). Methane oxidation in sediment and water column environments—Isotope evidence. *Organic Geochemistry*, *10*(4–6), 759–768. https://doi.org/10.1016/S0146-6380(86)80013-4

Zhang, R., Jiang, T., Tian, Y., Xie, S., Zhou, L., Li, Q., & Jiao, N. (2017). Volcanic ash stimulates growth of marine autotrophic and heterotrophic microorganisms. *Geology*, *45*(8), G38833.1. https://doi.org/10.1130/G38833.1

Zhao, B., Yao, P., Bianchi, T. S., Shields, M. R., Cui, X. Q., Zhang, X. W., et al. (2018). The Role of Reactive Iron in the Preservation of Terrestrial Organic Carbon in Estuarine Sediments. *Journal of Geophysical Research: Biogeosciences*, *123*(12), 3556–3569. https://doi.org/10.1029/2018JG004649

Zonneveld, K. A. F., Versteegh, G. J. M., Kasten, S., Eglinton, T. I., Emeis, K. C., Huguet, C., et al. (2010). Selective preservation of organic matter in marine environments; Processes and impact on the sedimentary record. *Biogeosciences*, *7*(2), 483–511. https://doi.org/10.5194/BG-7-483-2010

Acknowledgements

This work was funded by a Natural Environment Research Council (NERC) grant, NE/K00543X/1, “The role of marine diagenesis of tephra in the carbon cycle”. T.M.G. acknowledges support from NERC grant, NE/R004978/1. Datasets for this research are available in the Supplementary Information, and on the Pangaea data archive (doi to follow once assigned)

Figures

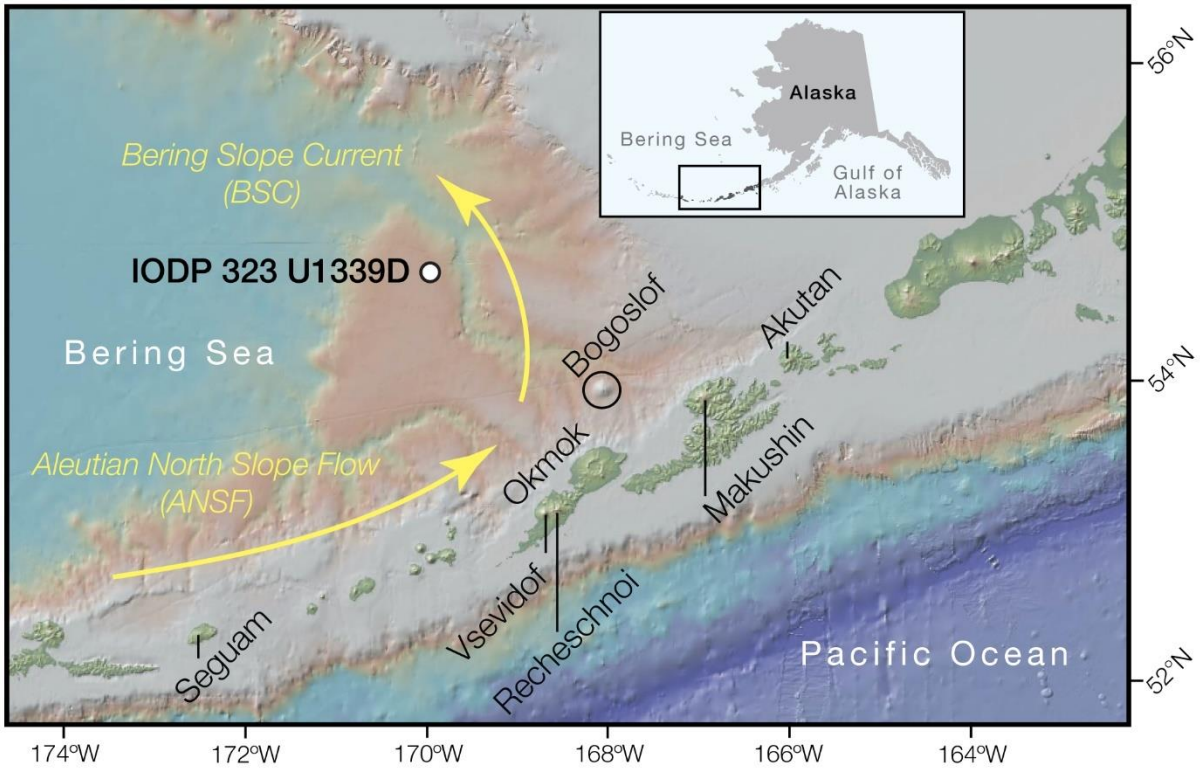

675

676 Figure 1: Map of part of the Aleutian Island Arc showing the location of IODP core U1339D. The inset
677 map shows the location of the sampling site within Alaska. Also shown are a number of volcanoes
678 which have actively supplied ash to the Bering Sea during the Quaternary Period (as defined by the
679 Global Volcanism Program of the Smithsonian Institution). Marked in yellow are the key ocean
680 currents affecting sedimentation at this site.

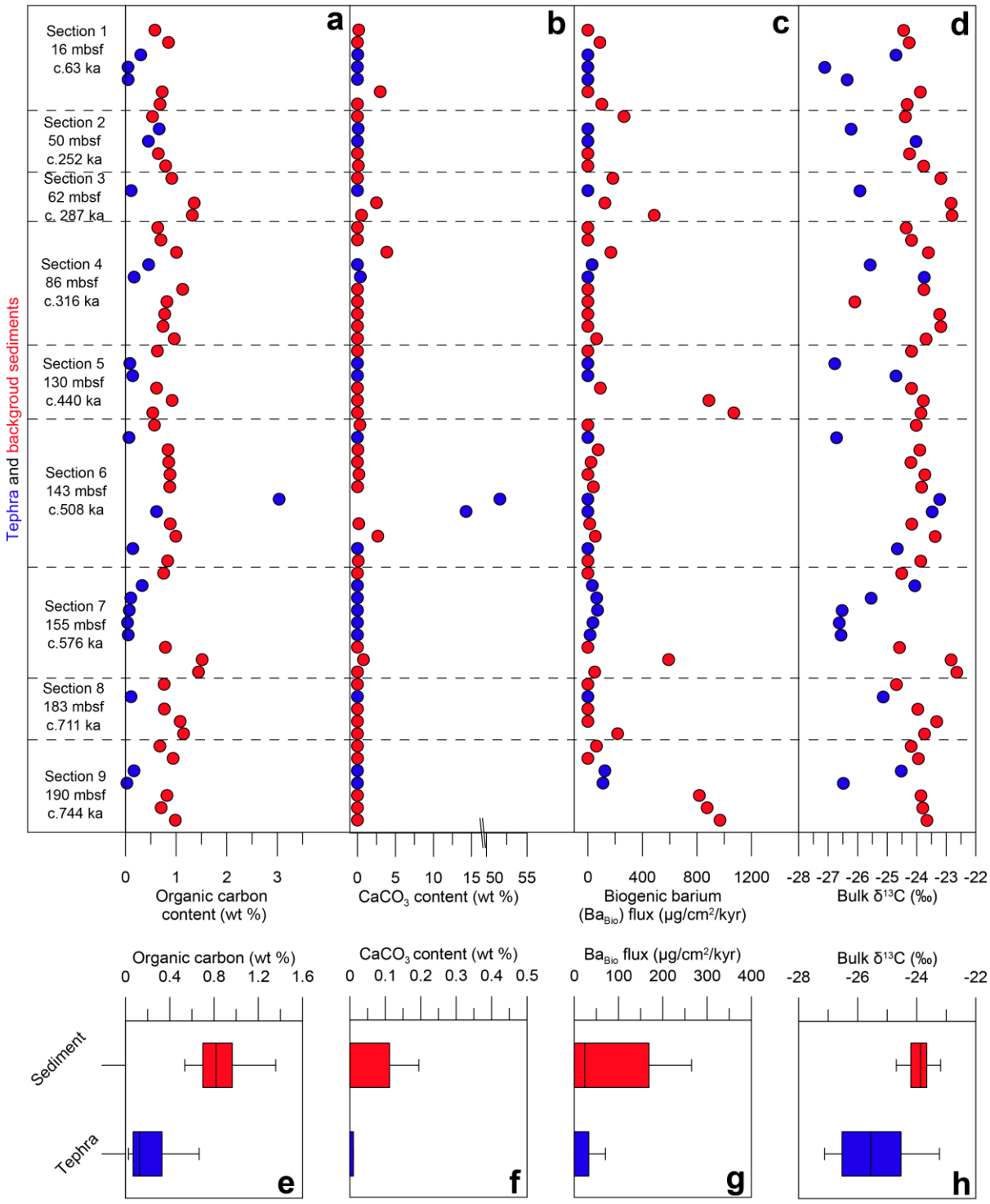

Figure 2: Geochemical parameters of tephra and background sediment from U1339D. a) Organic carbon content in tephra (purple) and background sediments (blue). b) $CaCO_3$ content, c) biogenic barium flux, d) bulk $\delta^{13}C$, with average value for both sample type indicated by solid lines. To the left of boxes a-d are the section numbers, depths in metres below sea floor (mbsf) and indicative ages in thousands of years before present (ka). Panels e-h display box and whisker diagrams of the data presented in panels a-d. Boxes are defined between the first and third quartile (interquartile range; IQR), with minimum and maximum whiskers representative of 1.5 times the IQR, and with any outliers (>1.5 times IQR) removed.

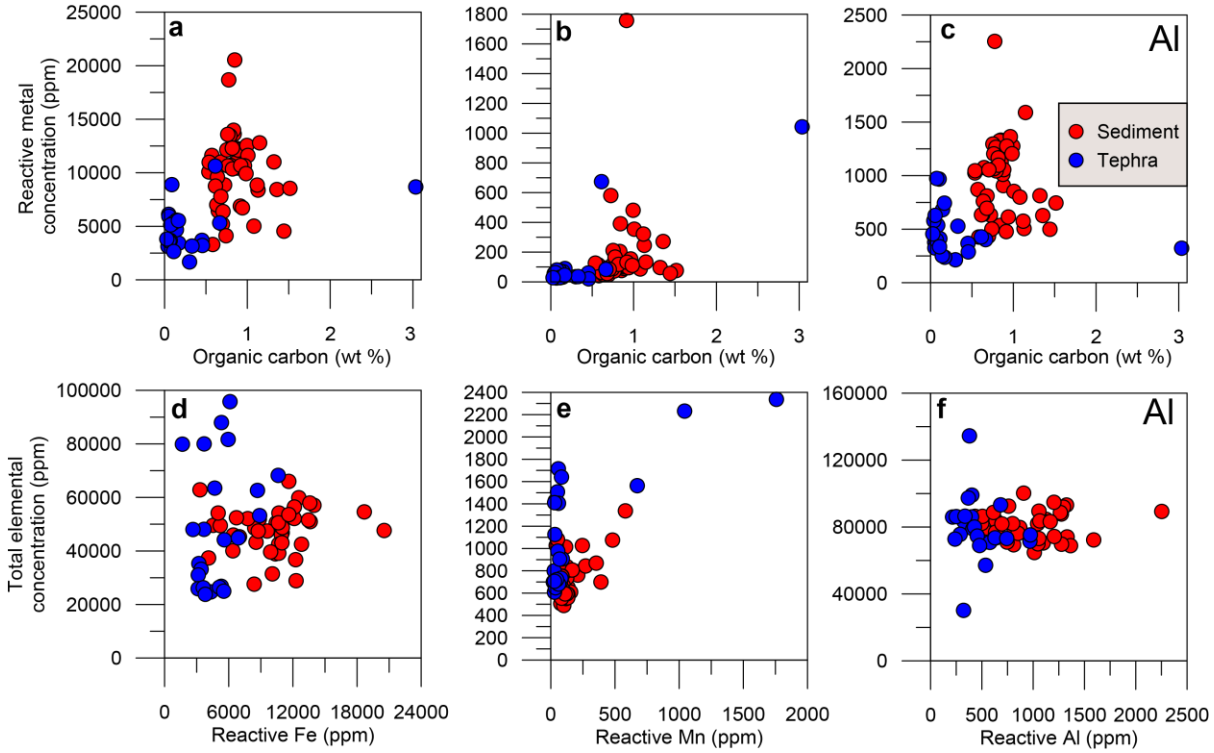

690

691 Figure 3: Comparison of total metal contents, reactive metal contents and organic carbon (OC)
692 content of sediments and tephras from Site U1339D. Panels a-c display reactive metal
693 concentrations plotted against OC whilst panels d-f show total elemental content for Fe, Mn and Al
694 against respective reactive metal content. Tephra samples are coloured blue, with sediments in red.

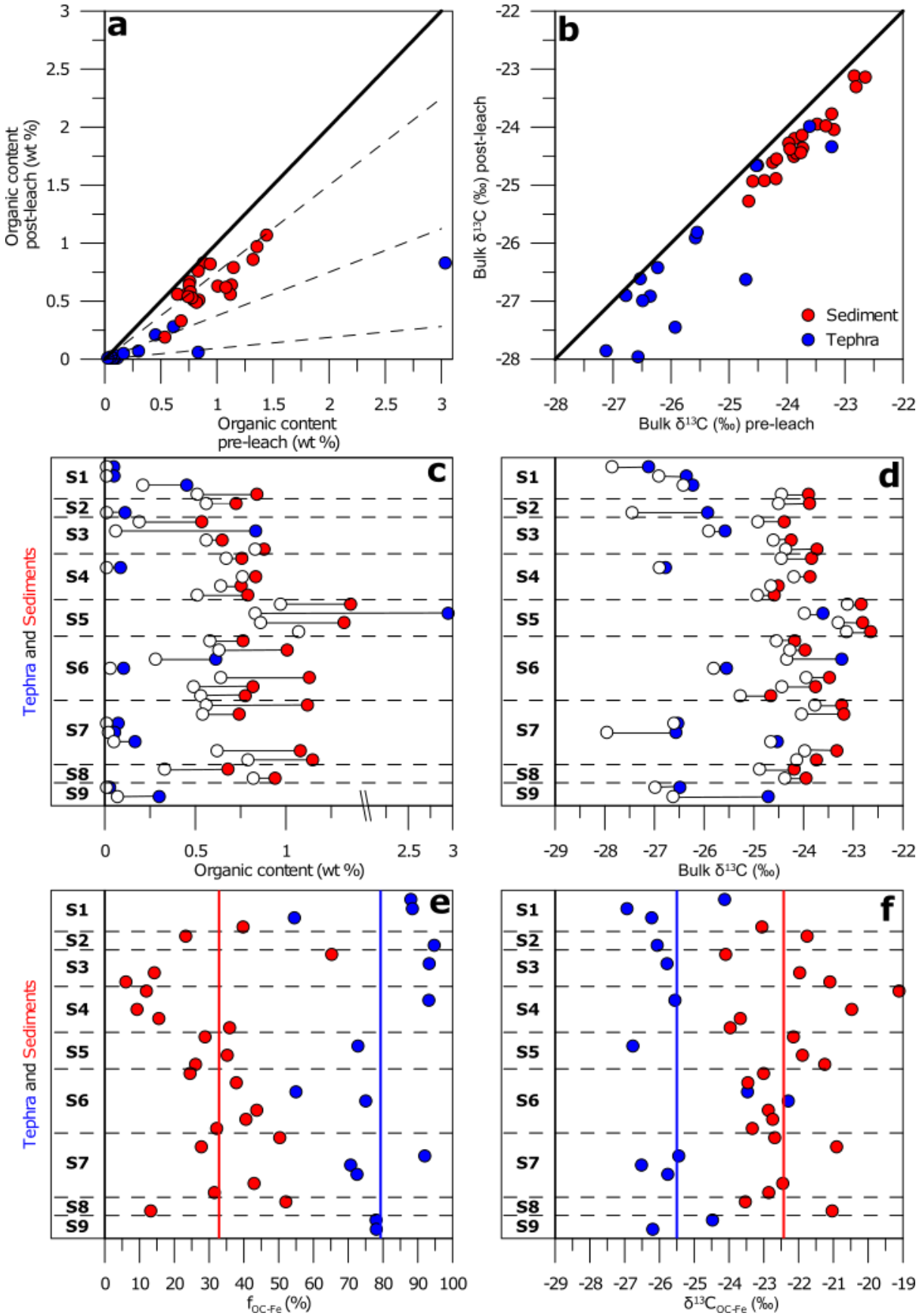

Figure 4: Results of dithionite extraction experiments. In all panels, tephras are indicated by blue circles and background sediments are in red. a) Organic carbon (OC) content in all samples before

extraction versus OC content after extraction. Thick black line indicates where samples should plot if no OC was extracted. Labelled dashed lines indicate the fraction of OC associated with reactive phases ($f_{OC\text{-}Fe}$). b) Plot of bulk $\delta^{13}C$ before and after extraction. Thick black line indicates where samples should plot if no isotopic change were observed. Panels c-d display the same data as a and b but indicate the shift from the original sample (filled circles) to extracted samples (open circles). e) $f_{OC\text{-}Fe}$, with thick lines indicating average $f_{OC\text{-}Fe}$ for tephra (blue) and sediment (red). f) Bulk isotopic composition of OC associated with reactive phases $\delta^{13}C_{OC\text{-}Fe}$. As before, thick coloured lines indicate the average $\delta^{13}C_{OC\text{-}Fe}$ of tephra (blue) and sediments (red). For panels c-f, section numbers are indicated to the left. These refer to the ages and depths indicated in Figure 2.

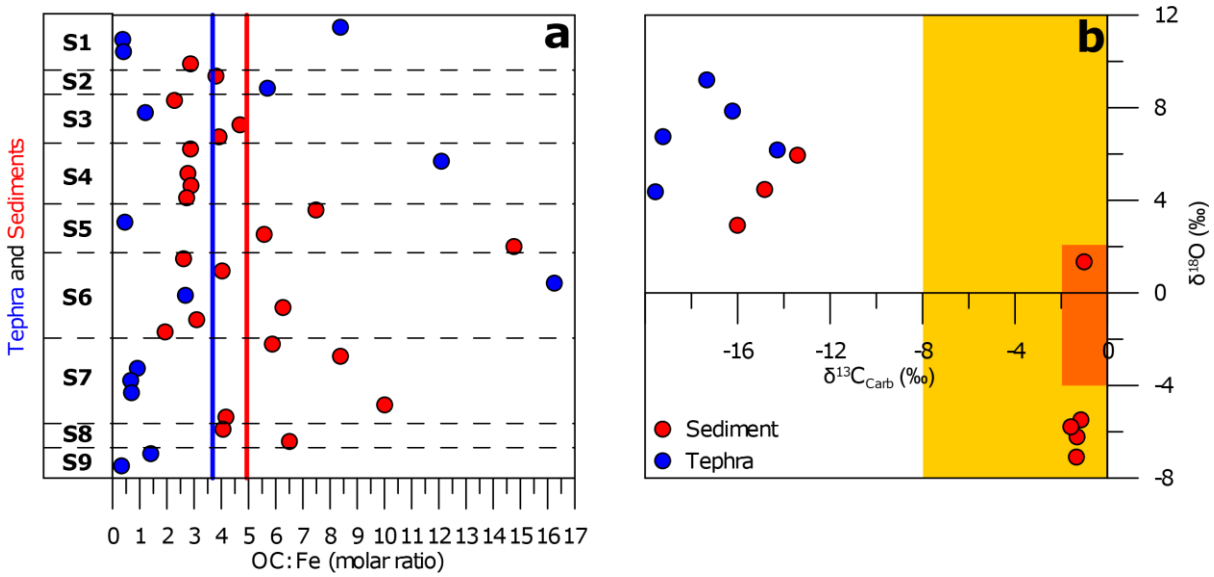

Figure 5: Geochemistry of tephras and sediments from Site U1339D. a) Ratio of OC to reactive Fe, using molar masses for sediments (red) and tephras (blue). b) $\delta^{13}C$ and $\delta^{18}O$ of the carbonate fraction (see Methods), with typical values for isotopic composition of seawater (orange rectangle) and biogenic carbonate (yellow rectangle) highlighted. For panel a, section numbers are indicated to the left. These refer to the ages and depths indicated in Figure 2.

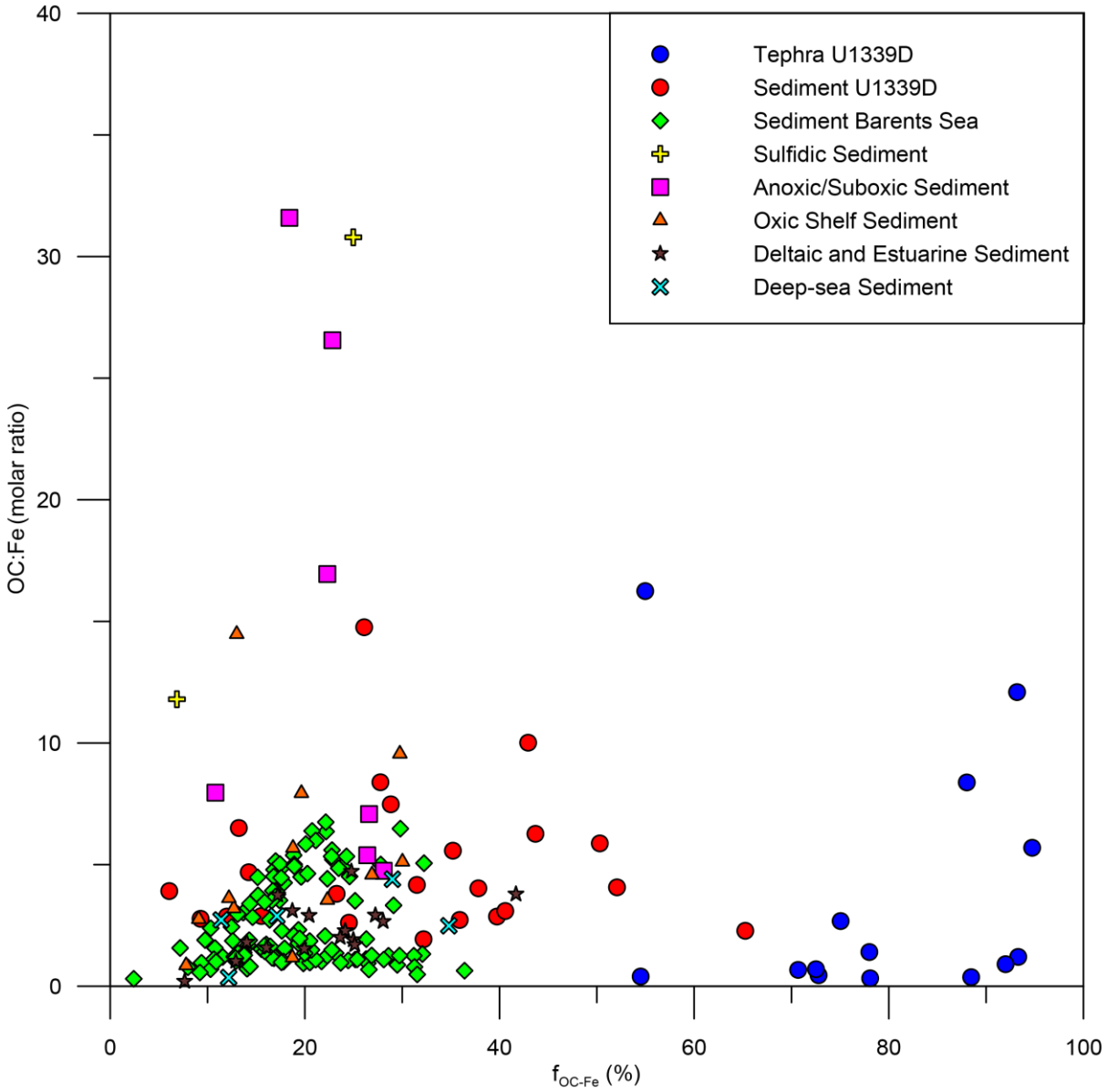

Figure 6: Comparison of the fraction of OC associated with FeR (f_{OC-Fe}) with the Fe:OC molar ratio from this study and a selection of previous studies. Data from this current study from tephras (blue circles) and sediments (red circles) are shown alongside sediment data from the Barents Sea (green diamonds; Faust et al., 2021). Also shown are data from the compilation of Lalonde et al., (2012), with samples from anoxic/suboxic environments (magenta squares), sulfidic sediments (yellow plus symbols), oxic shelf sediments (orange triangles), deltaic and estuarine sediments (brown stars) and deep-sea sediments (cyan crosses).

Tables

Table 1: Summary of experimental results. Mean, minimum and maximum values for each of the measured variable are presented, for both tephra and sediment layers.

Tephra Layers			
	Mean	Minimum	Maximum
Before dithionite extraction			
Organic carbon content (wt%)	0.33	0.03	3.03

Inorganic carbon content (wt%)	3.02	0	51.66
Ba_{Bio} flux (mg cm^{-3} kyr)	201	0	2682
Total Fe (wt%)	4.8	2.38	9.58
Total Mn (ppm)	1082	608	2232
Total Al (wt%)	7.98	3.02	13.4
Bulk $\delta^{13}C$ (‰)	-25.4	-23.23	-27.12
After dithionite extraction			
Organic carbon content (wt%)	0.12	0.01	0.83
Reactive Fe (wt %)	0.57	0.32	1.06
Reactive Mn (ppm)	175	19.83	1042
Reactive Al (ppm)	524.92	287.8	972.8
Bulk $\delta^{13}C$ (‰)	-26.29	-23.99	-27.96
$f_{OC\text{-}Fe}$ (%)	0.79	0.55	0.95
$\delta^{13}C_{Fe\text{-}OC}$ (%)	-25.83	-23.39	-24.16

Sediment Layers

	Mean	Minimum	Maximum
Before dithionite extraction			
Organic carbon content (wt%)	0.84	0.15	1.41
Inorganic carbon content (wt%)	0.33	0	3.86
Ba_{Bio} flux (mg cm^{-3} kyr)	166	0	1071
Total Fe (wt%)	4.8	2.88	6.6
Total Mn (ppm)	784.8	488.4	2337
Total Al (wt%)	8.04	6.47	10.03
Bulk $\delta^{13}C$ (‰)	-23.82	-22.65	-24.71
After dithionite extraction			
Organic carbon content (wt%)	0.61	0.07	1.07
Reactive Fe (wt %)	0.98	0.17	1.87
Reactive Mn (ppm)	170.8	34.32	580.5
Reactive Al (ppm)	914.42	214.4	2254
Bulk $\delta^{13}C$ (‰)	-24.37	-23.99	-27.96
$f_{OC\text{-}Fe}$ (%)	0.33	0.06	0.78
$\delta^{13}C_{Fe\text{-}OC}$ (%)	-24.16	-22.94	-26.39

725